Applied Catalysis B: Environmental 235 (2018) 197–206

Contents lists available at ScienceDirect

Applied Catalysis B: Environmental

journal homepage: www.elsevier.com/locate/apcatb

Photocatalytic NH_3 *versus* H_2 evolution over g-C_3N_4/Cs_xWO_3: O_2 and methanol tipping the scale

Anye Shi[a,1], Huihui Li[a,*,1], Shu Yin[b], Zaili Hou[a], Jiayue Rong[a], Jiachi Zhang[a,*], Yuhua Wang[a]

[a] National & Local Joint Engineering Laboratory for Optical Conversion Materials and Technology, School of Physical Science and Technology, Lanzhou University, 222 South Tianshui Road, Lanzhou 730000, PR China

[b] Institute of Multidisciplinary Research for Advanced Materials, Tohoku University, 2-1-1 Katahira, Aoba-ku, Sendai 980-8577, Japan

ARTICLE INFO

Keywords:
Photocatalysis
N_2 fixation
H_2 evolution
O_2 content
Sacrificial agent

ABSTRACT

Cs_xWO_3 nanorods can be used to sensitize the single layer g-C_3N_4, where full spectrum light harvesting excited electrons to drive the photocatalytic reduction of N_2 into NH_3. Under UV light, both water splitting and solar ammonia synthesis reaction exhibit high activity. However, selectivity towards ammonia over hydrogen is realized under NIR irradiation. With the control of methanol, O_2 can directly decide the NH_3 or H_2 evolution on photocatalyst. The origin is the strong capture of O_2 with the electrons from the photocatalyst under light irradiation to yield the oxygen active species, which transfer electrons subsequently with help of methanol to generate NH_3. However, H_2 production will be suppressed by O_2. And with its sacrifice, methanol preserves the produced NH_3 from oxidation. The O_2-sacrificial agent mediated NH_3 evolution reaction found here provides insights in the promotion role of them in other catalysis.

1. Introduction

Solar driven nitrogen fixation has been considered to be a promising method to replace the traditional Haber-Bosch process, since the pioneering work reported by Schrauzer and Guth on the study of photocatalytic N_2 fixation over titania based catalysts [1]. However, the wide band gap of titania based semiconductor, the poor interaction between catalyst and N_2 molecules, and the high energy N_2 intermediates make it difficult to perform photocatalytic N_2 fixation [2]. Specially, the sufficient N_2 activation, the prerequisite of its reduction, is crucial. The nitrogen fixation results are not satisfactory.

Recently, localized surface plasmon resonance (LSPR) of metallic nanostructures has received much attention because of its light-harvesting and electric-field-enhancing effects [3]. It reported that the conversion selectivity of N_2 into NH_3 could be improved through plasmon-induced charge separation over a Au/Zr/$SrTiO_3$ catalyst [4]. In addition, efficient N_2 photoreduction to NH_3 has been achieved over oxygen vacancies introduced BiOBr nanosheets or nitrogen vacancies doped g-C_3N_4 [5]. The research results indicated that the improved N_2 photofixation abilities were benefited from enhanced N_2 activation and promoted interfacial electron transfer. Then, other surface defects also show a similar effect on nitrogen photofixation, such as Fe^{3+} doping in g-C_3N_4 and oxygen vacancies doped BiOCl [6].

It is known that g-C_3N_4 has limitation to drive water oxidation and needs sacrificial electron donors such as alcohols [7]. The promotion of water oxidation will benefit providing sufficient H^+ for N_2 reduction, and then the efficiency of NH_3 generation is improved [7]. Fortunately, WO_3-based semiconductors are considered to be good at water oxidation due to their proper band structure [8]. Therefore, due to the outstanding electron and proton conductivity, herein g-C_3N_4 and Cs_xWO_3 was selected to form a g-C_3N_4/Cs_xWO_3 (CW) nanocomposite as the photoactive material to explore the N_2 photofixation. Unique N_2 reduction to ammonia was achieved by CW composite under NIR light irradiation. Careful studies evidently revealed the indispensable roles of g-C_3N_4 and Cs_xWO_3 in electron transfer and photo-induced protonation. Furthermore, by studying the LSPR assistance strategy, a possible mechanism of the nitrogen photofixation was proposed and the selectivity between hydrogen and ammonia generation was also discussed.

2. Experimental

All chemicals were purchased from Aladdin Chemical Reagent Co., Ltd. and used as received without further purification.

2.1. Preparation of single layered g-C_3N_4

Single layer g-C_3N_4 was prepared by the protonation treatment of

* Corresponding authors.
E-mail addresses: lihh@lzu.edu.cn (H. Li), zhangjch@lzu.edu.cn (J. Zhang).
[1] These authors are co-first authors.

https://doi.org/10.1016/j.apcatb.2018.04.081
Received 4 February 2018; Received in revised form 10 April 2018; Accepted 30 April 2018
Available online 01 May 2018

bulk g-C_3N_4 from the thermal polycondensation of melamine [9]. First, 1.60 g of melamine was heated at 550 °C for 3 h. Then, 1 g bulk one was dispersed in 5 ml HCl (37%) for 24 h. After centrifugation, washing and drying, the final single layer g-C_3N_4 particles were obtained.

2.2. Preparation of Cs_xWO_3

Nanosized Cs_xWO_3 was prepared by a solvothermal process [10]. WCl_6 ethanol solution and CsOH ethanol solution were mixed with a nominal Cs/W atomic ratio of 0.5 to form precursor solution. Then, after the solvothermal reaction, the final Cs_xWO_3 was obtained after centrifugation, washing and drying.

2.3. Fabrication of g-C_3N_4/Cs_xWO_3 (CW) compounds

According to the differences in the surface electrical behaviour of protonated g-C_3N_4 and Cs_xWO_3, it is easy to fabricate a uniform hybrid by electrostatic attraction in aqueous solution [11]. 0.5 g Cs_xWO_3 and 2.0 g of as-prepared single layer g-C_3N_4 were added into 100 ml of deionized water and then treated by ultrasonication for 4 h. The powder product was separated by centrifugation, and then vacuum dried at 60 °C overnight.

2.4. Characterization

X-ray diffraction (XRD) characterizations were performed on a Shimadzu XRD-6000 powder X-ray diffractometer with CuKa radiation. The FT-IR spectra were recorded using a VERTEX 70 V/80V Fourier transformed infrared spectrometer (Bruker, Germany) by means of the KBr pellet technique. The UV/VIS diffuse reflectance spectra were obtained on a Perkin-Elmer Lambda 950 UV/VIS spectrometer equipped with Labsphere integrating over the spectral range of 250–1600 nm. Transmission electron microscopy (TEM), and high-resolution TEM (HRTEM) images were obtained with a JEOL JEM-2100 microscope at 200 kV. X-ray photoelectron spectroscopy (XPS) and ultraviolet photoelectron spectroscopy (UPS) measurement was done using a Kratos AXIS Ultra DLD XPS system, all the binding energies were referenced to the C1s peak at 284.6 eV of the surface adventitious carbon. The specific surface areas were measured out by the BET method (Micromeritics Instrumetns, TriStar α3020). Electron spinning resonance (ESR) was measured by JES-FA300. Photocurrents were measured using an electrochemical analyzer (CHI 660b) in a standard three-electrode system using the prepared samples as the working electrodes with an active area of ca. 1.00 cm × 1.00 cm, a Pt sheet and an Ag/AgCl (saturated KCl) electrode were used as the counter electrode and reference electrode, respectively. A 0.1 M Na_2SO_4 solution was used as the electrolyte. Ar and N_2 were introduced into reactor respectively. The electrochemical impedance spectroscopy (EIS) was measured at −1.4 V (vs. RHE) in 0.5 M Na_2SO_4 solution, and the perturbation signal was 5 mV with the frequency ranged from 0.1 Hz to 100 kHz. Atomic force microscopy (AFM) analysis was performed by Agilent 5500 ILM. A Vario EL cube was employed to carry out elementary analysis and an IRIS ER/S was used to determine element content via inductively coupled plasma atomic emission spectroscopy (ICPAES).

Optical spectra of the Cs_xWO_3 were measured in tetrachloroethylene (TCE), dimethylformamide (DMF), and acetonitrile (MeCN) solution on a Perkin-Elmer Lambda 950 UV/VIS spectrometer equipped with Labsphere integrating over the spectral range of 250–1600 nm.

Determination of NH_4^+ cations by ion chromatography (IC) method was achieved by using a Dionex ICS-1500 ion chromatograph (Dionex, Sunnyvale, CA, USA). The chromatographic system consisted of an advanced gradient pump and a DS-6 conductivity detector. Chromatographic separations on a Dionex IonPac®-CS12 cation exchanger was performed using a cation Self Regenerating Suppressors (CERS 4 mm) with a flow rate of 1.0 ml/min. The injection volume was 25 µl for each sample. Rotary evaporation operation was conducted to remove methanol from the reaction solution.

2.5. LC–MS analysis

Indophenol method based on the LC–MS was used to determine the quantitative of NH_3 generation [6]. The reaction solution was injected directly for analysis. All the products were investigated in ESI (positive ion mode) on an Ultimate 3000-TSQ (LCMS-ESI).

2.6. Photocatalytic N_2 fixation

Typically, 20 mg of sample was dispersed in an aqueous solution (40 ml) containing 10 vol. % methanol as an electron donor. 3 wt% platinum was used as a cocatalyst. Prior to irradiation, the reaction solution was sealed by a silicone stopper, and subsequently flushed with dry N_2 in both of solution and atmosphere to remove O_2 completely. In comparison, the experiments were also carried out with dissolving O_2 in solution or air condition. NH_3 yield was determined via a colorimetric method using Nessler reagent as an indicator [5]. Typically, 1.5 ml reaction solution was added to 1 ml of KOH (0.25 M) and then mixed thoroughly with 0.25 ml 0.2 M $KNaC_4H_4O_6$ and 0.25 ml Nessler reagent. The mixed solution incubated for 20 min at room temperature. The absorbance of the solution at 425 nm was measured by the UV/VIS spectrometer. The calibration curves are shown in Fig. S9a.

The active species generated in the photocatalytic N_2 fixation process could be detected through trapping by 5.0 mg of $AgNO_3$, isopropyl alcohol (IPA), ammonium oxalate (AO) or benzoquinone (BQ).

2.7. Photocatalytic H_2 or O_2 evolution

To determine the evolved hydrogen or oxygen, a calibrated Varian GC-3380 Gas Chromatograph equipped with a thermal conductivity detector was employed using Ar as the carrier gas as our previous work [9]. Hydrogen production was carried out by dispersing 50 mg of as-prepared sample in an aqueous solution (100 ml) containing 10 ml of the 10 vol % sacrificial agent as an electron donor. 3 wt% platinum was used as a cocatalyst. Oxygen production was performed by dispersing the same amount of sample but in an aqueous $AgNO_3$ solution (0.01 M, 100 ml). For pure water splitting, 3 wt% platinum was used as a cocatalyst and 0.005 M of NaI was added as a redox mediator.

2.8. Photoelectrochemical N_2 fixation

All the electrodes and experimental conditions are the same as the photocurrent measurement, except for inducing 10 vol. % methanol as a electron donor in the sealed chamber. Before irradiation, N_2 was introduced into reactor for 20 min. The NH_3 and H_2 yields were detected as the same methods above.

2.9. Light source

(a) a full spectrum LED lamp (365–940 nm) with the intensity of 100 mW/cm^2;
(b) a series of monochromatic LED lamp (365, 395, 405, 425, 850, 940 nm) with the same intensity of 20 mW/cm^2.

2.10. Theoretical Calculation

All the calculations for pristine g-C_3N_4 and V-rich g-C_3N_4 were carried out using density functional theory (DFT) calculations with ωB97X-D/6-31G(D)* basis setting for both geometry optimization and frequency calculation on Gaussian09 program. The ωB97X-D functional is a long range dispersion-corrected functional and is good for non-covalent interactions [28]. Energies of respective surface bound intermediates and free molecules are corrected by the corresponding zero-point energy. For more details, please see the data in Table S5.

2.11. Apparent quantum yield calculations

The apparent quantum yield (AQY) for the NH_3, H_2 and O_2 evolution was determined under 20 mW/cm^2 monochromatic light irradiation. The AQY was calculated as:

$$AQY = \frac{N_e}{N_p} \times 100\% = \frac{NMN_A hc}{SPt\lambda} \times 100\%$$

where *N*e is the amount of reaction electrons, N_p is the amount of incident photons, N_A is Avogadro's constant, h is the Planck constant, c is the speed of light, S is the irradiation area, P is the intensity of the irradiation, t is the irradiation time, and λ is the wavelength of the monochromatic light. For the AQY of H_2, NH_3 and O_2, the *NM* represent for 2 M(H_2), 3 M(NH_3) and 4 M(O_2) [6].

3. Results and discussion

For the first time, a uniform hybrids of g-C_3N_4 and Cs_xWO_3 was obtained by electrostatic attraction in aqueous solution. Single layer g-C_3N_4 nanosheets with abundant N vacancies and O dangling bonds were exfoliated by protonation [9]. Oxygen vacancies rich Cs_xWO_3 nanorods were synthesized through hydrothermal method [10]. CW composites were fabricated by self assembly, owing to the opposite surface electrochemical properties [11]. As shown in the TEM image (Fig. S1a1-3), Cs_xWO_3 nanorods are dispersed on the surface of single layer g-C_3N_4 nanosheets. AFM measurement confirms that the thickness of the single nano-layer g-C_3N_4 under study is about 0.5 nm (in Fig. S1b1-3). The use of single nano-layer g-C_3N_4 is convenient to improve the separation of electron-hole pairs in it. It is known that the SPR is sensitive to the refractive index (RI) of solvent and there is a linear relationship between the solvent RI and the plasmon peak position [12]. The optical spectra of Cs_xWO_3 were collected in tetrachloroethylene (TCE), dimethylformamide (DMF), and acetonitrile (MeCN), with respective RIs of 1.51, 1.43, and 1.35. There is an obvious and systematic shift of the peak position to a longer wavelength with the solvent RI increases (Fig. S1c). The results from the insert plot of RI versus peak wavelength further indicates the plasmon resonance absorption [13].

As indicated by XRD pattern (Fig. S2a), the characteristic peaks belonged to the hexagonal phase of cesium tungsten bronze (JCPSD No. 831334) are all presented in the XRD pattern of CW composite without any impurity peak. The (002) peak of g-C_3N_4 should be overlapped by the peak at ~27.4° of Cs_xWO_3. FT-IR spectra show no extra impurity peak between pure g-C_3N_4 or Cs_xWO_3 and CW composite (Fig. S2b). The peaks at 674 and 972 cm^{-1} can be ascribed to the W—O—W and W═O bonds respectively, suggesting the presence of W metal with different valence [14]. XPS was further used to investigate the chemical composition of CW sample (Fig. S3). O 1s spectra (Fig. S3a) of all samples exhibit two same peaks, one at ca. 532.7 eV caused by the adsorbed H_2O and another one at ca. 531.7 eV attributed to the surface hydroxyl group [15]. One additional peak for CW and Cs_xWO_3 at ca. 530.2 eV can be ascribed to the W—O bond [16]. CW composite shows a stronger peak at 531.7 eV and a weaker peak at 532.7 eV similar to those in g-C_3N_4, while the 532.7 eV peak is stronger than the 531.7 eV peak in Cs_xWO_3. The increase of hydroxyl group is originated from g-C_3N_4 constituent, confirming that CW has been fabricated instead of simple mixture.

Since vacancies may play an important role in photocatalytic N_2 reduction process [6], besides XPS, ESR analysis was also performed (Figs. S3 and S4). The peaks at 287.8 and 288.2 eV are ascribed to C-N_2 and C-N_3 in C1s spectra (Fig. S3b). C-N_2 peak is much weaker and C-N_3 peak even disappears after protonation, indicating the planar destruction. In N 1s spectra (Fig. S3c), C—N—C peak becomes much weaker and N-C_3 peak also disappears after protonation, suggesting N lost in tri-s-triazine rings. The sharp peak with g = 2.0034 also confirms the vacancies in the protonated g-C_3N_4 (Fig. S4) [17]. In W 4f spectra (Fig. S3d), Cs_xWO_3 and CW show W^{5+} and W^{6+} peaks, owing to oxygen vacancies [11]. The partial oxidation of CN after protonation results in O adsorption and O dangling bonds on the surface of g-C_3N_4 [9]. Replacing N with O promotes the positive electricity of C, benefiting the N_2 adsorption and the N—N triple bond weakening [18]. Furthermore, the protonation brings hydroxyl and carboxyl to the surface of catalysts. The hydroxyl or carboxyl could act as a proton donor in the reaction and then greatly improves the N_2 conversion efficiency [19].

DRS spectra were measured to evaluate the optical absorption ability of as-prepared samples (Fig. S5a). CW shows a wide range of light absorption from UV, Vis to the whole NIR region, indicating its potential in full-spectrum light driven catalytic reaction. The band gaps are estimated from the tangent lines in the plots of the square root of the Kubelka-Munk functions against the photon energy [20]. The result (Table S1) shows that the band gap energy increases from 2.88 to 2.92 then to 3.21 eV with increasing the Cs_xWO_3 content from g-C_3N_4 to CW then to Cs_xWO_3. Ultraviolet photoelectron spectra (UPS) were then carried out to determine the relative valence band maximum (Fig. S5b). The valence band edges of g-C_3N_4, CW and Cs_xWO_3 are 2.21, 2.46 and 2.98 eV. Thus, the calculated conduction band edges are −0.67, −0.46 and −0.23 eV. Their specific surface area values are almost the same as ca. 35 m^2/g (Table S1), indicating that surface area should not be the key factor.

Initial studies on the photocatalytic activity for N_2 fixation over as-prepared samples were carried out by irradiating with a full-spectrum lamp, using water as the reactant and proton source and 10% methanol as the electron donor. As shown in Fig. 1a, a large amount of NH_3 (813 μmol L^{-1}) can be generated over CW in N_2 atmosphere, while the NH_3 yields of g-C_3N_4 and Cs_xWO_3 are 304 and 63 μmol L^{-1} after 5 h, respectively. The full-spectrum light induced NH_3 generation rate is estimated to be 331 μmol h^{-1} per one gram of catalyst of CW, 2.6 and 14.4 times higher than g-C_3N_4 and Cs_xWO_3 (125 and 23 μmol h^{-1} g^{-1}). After cycling test, no significant photoreactivity decrease is observed, indicating the photo-stability of CW for ammonia synthesis (Fig. S6a).

H_2 and NH_3 generation selectivity is also investigated. As shown in Fig. S6b, under full-spectrum light irradiation, the H_2 evolution rates of g-C_3N_4, Cs_xWO_3 and CW are 831, 83 and 1544 μmol h^{-1} g^{-1}, which are 6.6, 3.6 and 4.7 times higher than their own NH_3 generation rate, respectively, suggesting that all samples exhibit a low overpotential for hydrogen evolution and a high overpotential for nitrogen reduction [21]. Besides the poor proton affinity of N_2, the N_2 reduction requires quite high reaction energy. The dissociation of N_2 triple bond needs the energy as high as 944 kJ/mol [22]. The conversion of N_2 to N_2H requires a large energy of 313.8 kJ/mol [6]. However, the splitting of H_2O to H_2 and O_2 needs only 237.2 kJ/mol [23]. Therefore, water splitting proceeds more easily than N_2 reduction.

To further study the selectivity over CW, the monochromatic light driven experiments were carried out (Fig. 1b, Table S2). Under UV light irradiation, it displays good activity in both NH_3 and H_2 generation. H_2 evolution rate is ca. 4 times higher than that of NH_3, indicating that UV light benefits for water splitting. However, N_2 reduction could be greatly promoted under NIR irradiation, since NH_3 generation rates are 1.1 μmol h^{-1} g^{-1} (850 nm) and 1.4 μmol h^{-1} g^{-1} (940 nm), 8 and 17 times higher than that of H_2. According to the material property, a plenty of excited electrons are generated in CW by UV light, while the NIR induced LSPR effect can only provide energy for limited hot electron and hole separation in Cs_xWO_3 component [24].

Water oxidation was also carried out in the 0.01 M $AgNO_3$ solution under UV–vis-NIR or monochromatic light source. Fig. 1c shows the oxygen production results over g-C_3N_4, Cs_xWO_3 and CW. Under full-spectrum light irradiation, the O_2 evolution rates of g-C_3N_4, Cs_xWO_3 and CW are 44.6, 224.6 and 266.5 μmol h^{-1} g^{-1} respectively. It is clear that after coupling Cs_xWO_3, CW exhibits excellent O_2 evolution activity 6 times higher than g-C_3N_4. Then, the water oxidation activity was also investigated under monochromatic light irradiation. As shown in

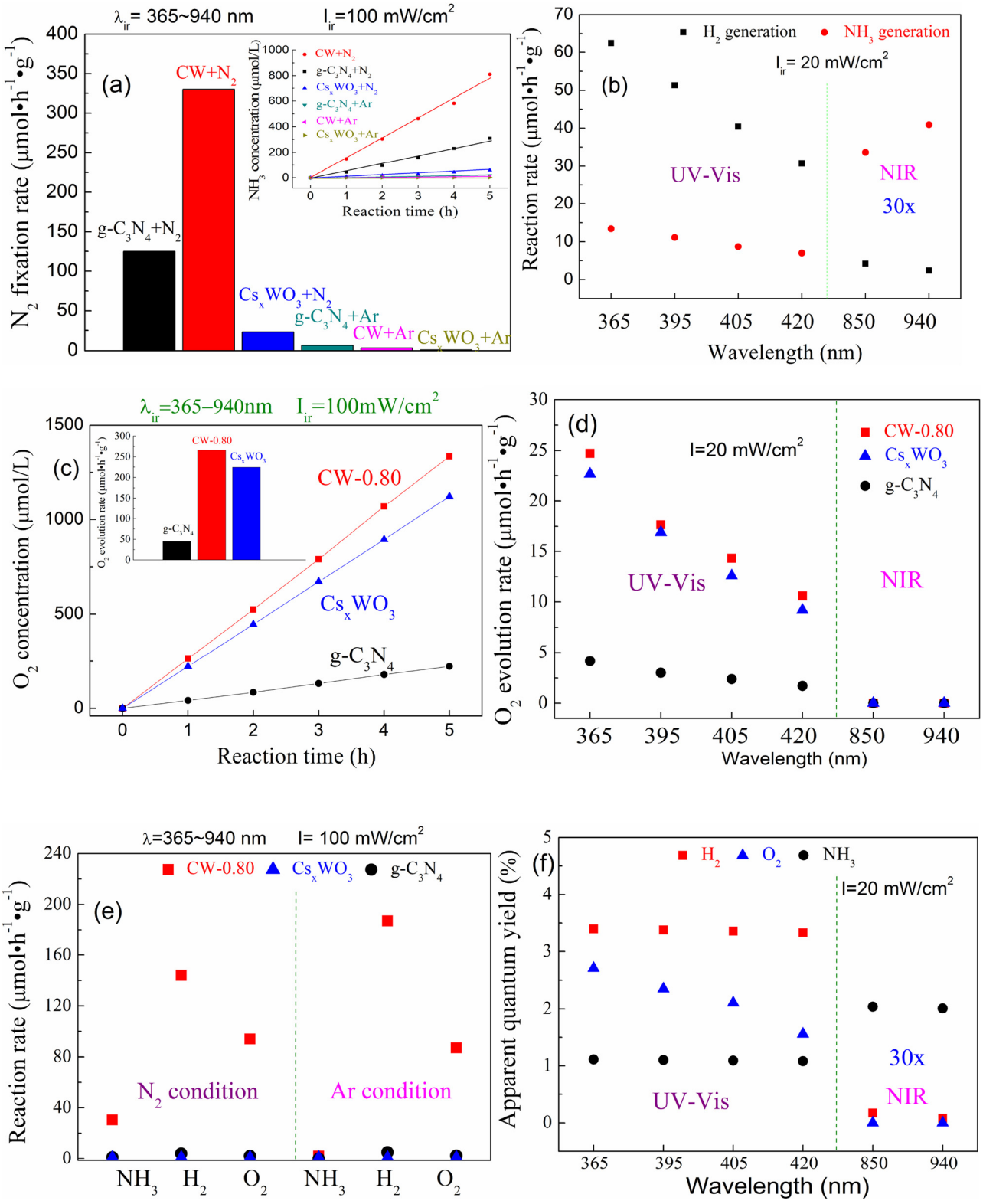

Fig. 1. (a) NH_3 production over Cs_xWO_3, g-C_3N_4 and CW under full spectrum light irradiation in N_2/Ar gas under O_2-free condition with 10% methanol. (b) NH_3 and H_2 generation rates over CW under UV or NIR monochromatic light under O_2-free condition with 10% methanol. (c) O_2 production over g-C_3N_4, Cs_xWO_3 and CW under UV–vis-NIR light irradiation. (d) O_2 generation rates over g-C_3N_4, Cs_xWO_3 and CW under monochromatic light irradiation. (e) NH_3, H_2 and O_2 generation rates over different samples with 3 wt% platinum in a 0.005 M NaI solution with N_2 or Ar under full spectrum light irradiation. (f) Apparent quantum yields of H_2, NH_3 and O_2 under different monochromatic light irradiation.

Fig. 1d, CW exhibits much higher O_2 evolution efficiency than g-C_3N_4 under UV light irradiation. However, no O_2 evolution was observed under NIR light irradiation, suggesting the lack of holes to drive water oxidation reaction.

Since CW is good at N_2 reduction and water oxidation, the photocatalytic NH_3, H_2 and O_2 generations in the pure water were further performed. The 3 wt% platinum was used as a cocatalyst and 0.005 M NaI was added as a redox mediator [25]. As shown in Fig. 1e, only CW shows high NH_3, H_2 and O_2 evolution rates under full-spectrum irradiation in N_2 atmosphere, the NH_3, H_2 and O_2 generation rates are 30.4, 144.1 and 94.2 $\mu mol\, h^{-1}\, g^{-1}$ respectively, indicating that the CW would act well in both reduction and oxidation reaction. However, in Ar atmosphere, the NH_3 or O_2 production decreased while the H_2 generation increased. The generation rates of NH_3, H_2 and O_2 are 0, 186.9 and 86.9 $\mu mol\, h^{-1}\, g^{-1}$. The generation ratio of H_2 to O_2 is ca. 2, also confirming the good pure water splitting activity of CW. In addition, no NH_3 generation in Ar atmosphere strongly confirms the crucial role of N_2 gas in NH_3 production.

Therefore, in Fig. 1f and Table S3, the apparent quantum yield (AQY) of the photocatalytic hydrogen evolution system over CW was determined to be 3.40, 3.38, 3.36 and 3.33% at 365, 395, 405 and 420 nm respectively. But, the AQY was quite low in NIR light region. Similar to H_2 generation, N_2 fixation exhibits the same AQY values under different UV light irradiation. The AQY of ammonia generation was 1.11, 1.10, 1.09, 1.08% at 365, 395, 405 and 420 nm. The AQY of ammonia generation is lower than that of hydrogen evolution, suggesting that UV light is positive for hydrogen evolution. However, the AQY of NIR light induced NH_3 generation was quite high. The AQY of ammonia generation were 0.068 (850 nm) and 0.067% (940 nm), 12 and 25 times higher than that of H_2 evolution under the same NIR light irradiation. Different from that of hydrogen or ammonia generation, the AQY value of O_2 evolution obviously decrease with the wavelength of light source increase in UV region. The AQY of O_2 evolution is 2.71, 2.35, 2.11 and 1.56% at 365, 395, 405 and 420 nm. No photocatalytic oxygen evolution was observed under NIR light irradiation. It is worth mentioning that the N_2 reduction was carried out under 365–940 nm light irradiation without additional sacrificial reagent or H_2 input. The as-prepared CW composite shows higher N_2 fixation ability than many other g-C_3N_4 or graphene based composite photocatalyst, as shown in Table S4.

It is well known that the photocatalytic water splitting for hydrogen evolution is achieved by photogenerated charge carriers [23]. It is easy for O_2 to capture electrons to form $\cdot O_2^-$, resulting in the H_2 generation decrease [23]. Therefore, for a large yield of H_2, O_2 is usually removed completely before the water splitting reaction takes place. On the other hand, electron transfer also plays an important role in the photocatalytic N_2 fixation. With the electron participation, both oxidation and reduction reactions can realize the N_2 fixation [1]. Since O_2 is a excellent electron acceptor, the performances of O_2 and its related free radicals should not be ignored.

To investigate the effect of O_2, the measurements of hydrogen and ammonia synthesis were carried out with different O_2 condition in a sealed chamber. As shown in Fig. 2a, with the O_2 content increase, there is a sharp decline in production of hydrogen. However, the yield of NH_3 is enhanced instead under the same condition. It suggests that O_2 plays a positive role in NH_3 formation. The influence of O_2 will further discussed after the study of the hole scavenger.

The presence of organic scavengers such as methanol will benefit for ammonia generation. It could obviously increase the NH_3 yield by means of methanol as an electron donor in the semiconductor [26]. In addition, methanol is also a superior •OH scavenger. With its sacrifice, methanol protects the produced NH_3 from further oxidation [26]. As shown in Fig. 2b, after adding methanol, a dramatic enhancement of nitrogen conversion rate can be observed, owing to the reduced charge combination. The system with 10% methanol addition could generate the largest amount of NH_3. But the further increase addition of methanol will cause an excessive expenditure of active species, resulting in a fewer NH_3 product. Adding 10% ethanol, the similar enhancement is achieved, though not as highly as methanol plays.

After going on to add different scavengers to the 10% methanol-reaction system, different N_2 fixation rates will be achieved. As shown in Fig. 3a, the $\cdot O_2^-$ scavenger (BQ) and ·OH scavenger (IPA) will bring a damage to the ammonia yield, suggesting the oxygen active species play an important role in the N_2 conversion. Then, a more serious declination is observed in the N_2 fixation rate, after adding another electron scavenger, $AgNO_3$. The sharp decrease caused by $AgNO_3$ indicates that electrons are crucial in the N_2 fixation. Compared with the results under the condition of oxygen dissolved in the solution, the absence of O_2 will results in a lower N_2 fixation rate, confirming O_2 and its active species play a positive role in the ammonia generation.

The effect of electron and O_2 on the hydrogen and ammonia generation was also studied under a LED light irradiation with the wavelength of 365 or 940 nm. As shown in Fig. 3b, the lack of electrons is a horror for both hydrogen and ammonia synthesis, since $AgNO_3$ has been added. The $\cdot O_2^-$ and ·OH scavengers will also reduce the generation rate. However, the presence of O_2 plays an entirely different role between H_2 and NH_3 evolution, which decreases the H_2 yield but improves the NH_3 generation. According to the above results, O_2 can improve the N_2 conversion, but it will injure the H_2 evolution seriously.

To elucidate the role of holes and O_2 in the catalytic reaction, the evaluation of ammonia and hydrogen generation rate was also carried out under different condition using a monochrome LED light. As shown in Fig. 4, after adding the hole scavenger methanol, the yields of both NH_3 and H_2 under different O_2 condition are greatly improved. Without the electron donor methanol, the yield of NH_3 or H_2 decreases with the O_2 content increase, owing to the electron expenditure. The $\cdot O_2^-$ and ·OH may oxidize NH_3 in the absence of sacrificial agent methanol. But, with the assistance of methanol, O_2 active species will release the electrons for catalytic reaction. The positive effect of O_2 active species under the methanol control has been confirmed in the above analysis (Fig. 3).

Under UV light (365 nm) irradiation, the presence of both O_2 and methanol shows a positive role in the enhancement of NH_3 generation, while O_2 harms the H_2 evolution seriously (Fig. 4a–b). For NH_3 synthesis, methanol has a much stronger influence than O_2. But the addition 20% methanol will cause an excessive expenditure of active species, resulting in a fewer NH_3 product than that of 10% methanol. However, under NIR light (940 nm) irradiation, the limited hot electrons and holes will be induced by LSPR effect only in Cs_xWO_3 component. The effect of methanol and O_2 on the N_2 conversion under NIR light is the same as that under UV light (Fig. 4c). For H_2 evolution, both the positive role of methanol and the negative role of O_2 are amplified (Fig. 4d). It is clear that the removal of O_2 will benefit for H_2 evolution, though the electrons are not enough. Therefore, the results indicate that without methanol, O_2 harms both hydrogen and ammonia evolution, while O_2 becomes a friend to the N_2 conversion with the assistance of methanol.

To further investigate the effect of O_2, the indophenol created in the reaction between NH_4^+ and phenolic-hypochlorite in different O_2 condition with the same 10% methanol under full-spectrum light irradiation was analyzed by LC–MS. As shown in Fig. 5a, a strong indophenol anion mass spectroscopy signal presents at 198 *m/z*, while a weak signal at 199 *m/z* also appears. The 199 *m/z* signal can be ascribed to the existence of $^{15}N_2$ in the atmosphere. It is clear that a much stronger signal can be observed with the existence of O_2, indicating again that O_2 plays an active role in the N_2 fixation.

The products created from N_2 fixation under different O_2 condition with the same 10% methanol was also analyzed by LC–MS. As shown in Fig. 5b, obviously, four peaks corresponding to the ion mass of $[HCHO + H]^+$, $[NH_2OH + H]^+$, $[CH_3OCH_3 + H]^+$ and $[NH_2NH_2 + H]^+$ can be observed. The former three are the •OH induced reaction products, while the last one generated from the electron reduction procedure. HCHO and CH_3OCH_3

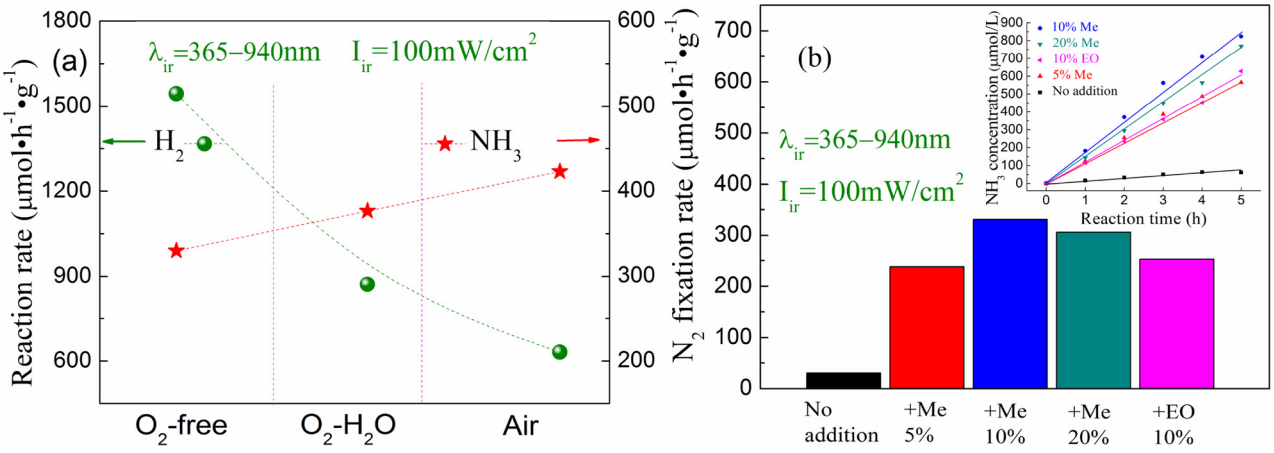

Fig. 2. (a) NH_3 and H_2 generation over CW photocatalyst under full spectrum light irradiation in 10% Me aqueous solution with different O_2 condition; (b) NH_3 production over CW composite with adding a different volume content of methanol or ethanol under O_2-H_2O condition. (Me: methanol, EO: ethanol).

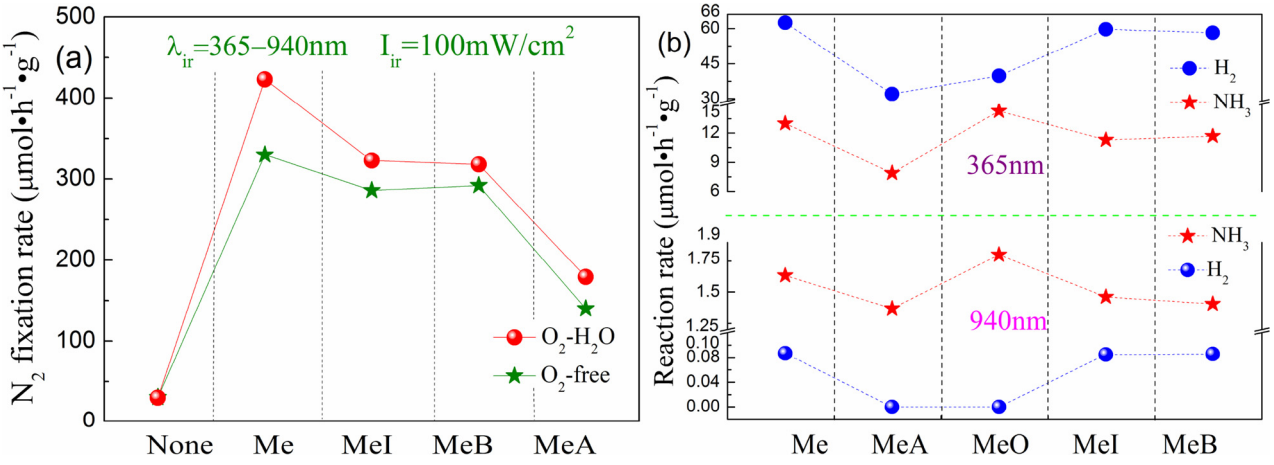

Fig. 3. (a) NH_3 production over CW under O_2-free or dissolved O_2 condition with different addition; (b) NH_3 and H_2 production over CW composite under UV or NIR monochromatic light with different addition. (Me: methanol, MeA: Me + AgNO3, MeI: Me + IPA, MeB: Me + BQ, MeO: Me + O_2-H_2O).

come from the oxidation of methanol, while NH_2OH can be attributed to the combination reaction of ·OH with ·NH_2 formed in nitrogen reduction process [26]. The signals of HCHO, NH_2OH and CH_3OCH_3 become stronger in the presence of O_2. No nitrite or nitrate signal appears, but the oxidation of methanol can be confirmed. It infers that the produced ammonia do not be oxidized with the presence of methanol. Therefore, it confirms that both O_2 and methanol play a key role in N_2 fixation.

Ion chromatography (IC) was also employed to determine the NH_4^+ concentration in the reaction solution. A 0.25 mM NH_4Cl solution was used as the standard. As shown in Fig. 5c, two peaks at 3.74 and 4.19 min can be observed, owing to the Na^+ from water and NH_4^+ respectively [27]. All the samples exhibit the signal peak at 3.74 min, which can be ascribed to the Na^+ containing in the pure water. However, no peak was observed at 4.19 min in the pure water or the dark reaction solution, indicating that the light irradiation was crucial in the NH_4^+ generation. Then, the reaction solution for CW, Cs_xWO_3 or g-C_3N_4 samples under 20 h full-spectrum light irradiation was analyzed. According to the calibration curve for NH_4^+ concentration using IC method (shown in Fig. S9b), the NH_4^+ production rate for CW is 137.7 μmol h^{-1} g^{-1}, 3.0 and 11.3 times higher than that of g-C_3N_4 and Cs_xWO_3 (45.8 and 12.2 μmol h^{-1} g^{-1}), which is similar to the results in Nessler colorimetric method. NH_4^+ production for CW samples under 200 h NIR or UV monochromatic LED light irradiation was also investigated (in Fig. 5d). NH_4^+ productions under NIR and UV are 0.51 and 5.4 μmol h^{-1} g^{-1} respectively, while the NH_4^+ generation for CW sample in the pure water under 20 h full-spectrum light irradiation is 16.1 μmol h^{-1} g^{-1}. The calculated NH_3 yield in IC and Nessler colorimetric method are listed in Table S5. Though the NH_3 yields in IC characterization are lower than those by using Nessler reagent, the relative NH_3 generation rates among different samples are the same between IC and Nessler reagent results.

To further investigate the products during N_2 fixation, maleic acid or extra N_2H_4 was added to the reaction solution (Fig. S6c, Table S6). Under light irradiation, N_2 reduction over CW is suppressed after adding the N_2H_2 scavenger maleic acid, indicating that N_2H_2 is an important intermediate. But the addition of oxalic acid without a C=C bond slightly suppressed the N_2 fixation efficiency of CW. Instead, an obvious enhancement of NH_3 generation is observed under both UV and NIR light irradiation after adding extra N_2H_4. Compared to the average growth rate of 2.5 times under UV light, a notable increase of NH_3 generation (9.7 times) is obtained under NIR irradiation. If any intermediate amount decreases or increases, the NH_3 yield will decrease or increase. More measurements were carried out under different temperature without light irradiation. As listed in Table S7, in the dark condition, with temperature rise, no NH_3 product was obtained, suggesting the importance of light irradiation. In addition, in the Ar atmosphere, all the photocatalysts including g-C_3N_4 show poor activities on N_2 conversion, even if under full-spectrum light irradiation (Fig. 1a). The slight amount of NH_3 may come from N_2 residues in Ar atmosphere. It confirms again that all the photocatalysts are stable during N_2 fixation. The NH_3 yields are 13.4 and 1.6 μmol/g h under 365 and 940 nm respectively. Interestingly, using these two monochrome LED lamp

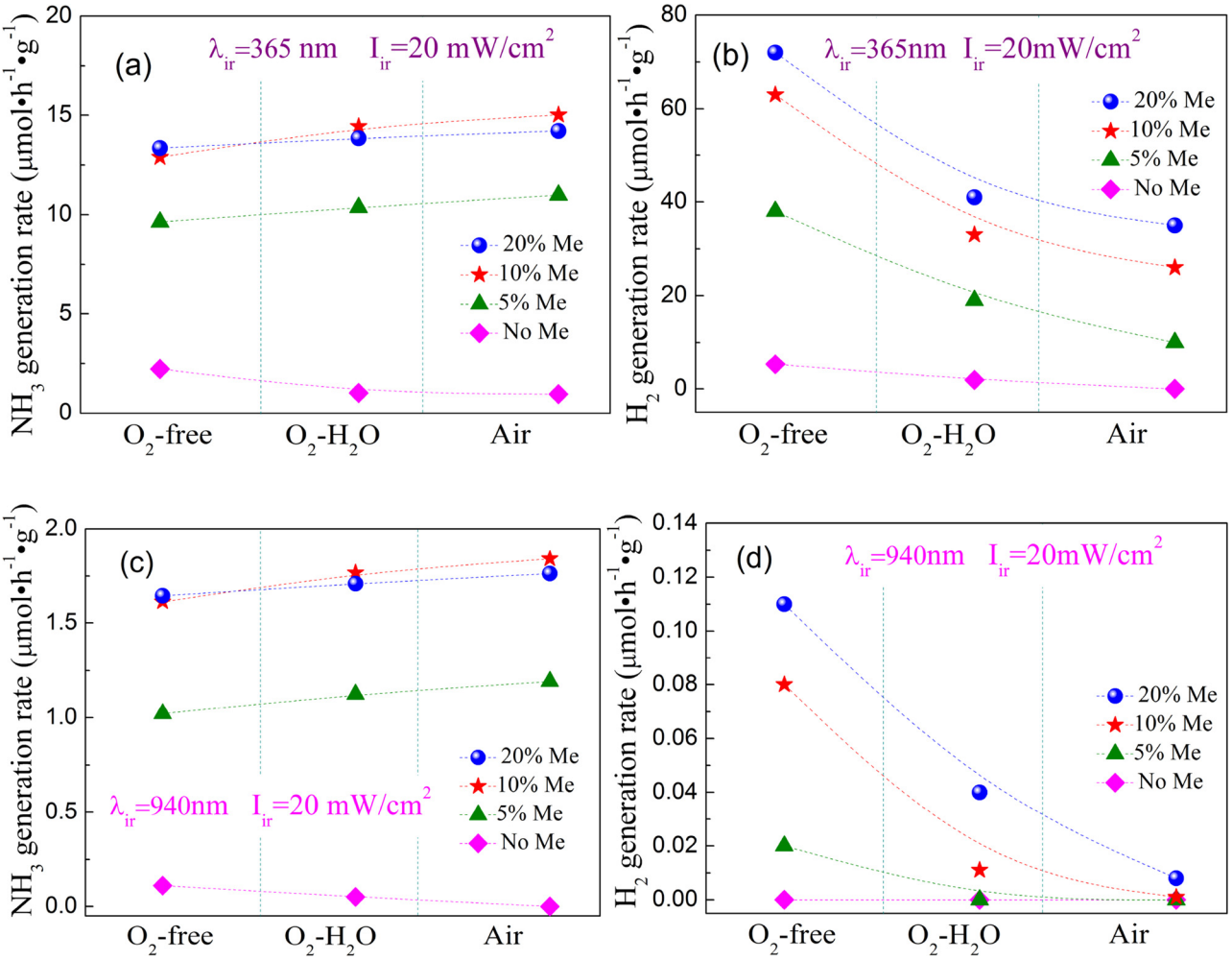

Fig. 4. (a,c) NH_3 and (b,d) H_2 production over CW composite under UV (365 nm) or NIR (940 nm) monochromatic light with different methanol.

simultaneously as the light source, 18 μmol/g h of NH_3 generation can be realized. The mixed light driven activity is improved greatly, 1.2 times higher than the result by adding up the UV and NIR induced activity values, indicating that a synergy effect is achieved. The LSPR effect can also provide extra excited state and active site [24]. Excited electrons can utilize the extra advantages and then efficiently activate N_2 fixation.

As indicated in Fig. 6a, the photocurrent response was tested in different atmosphere. In Ar gas, the photocurrent for CW reaches up to 3.0 μA/cm^2, while 1.0 μA/cm^2 in N_2 saturated atmosphere, suggesting that the photoelectron can be absorbed by N_2 [28]. EIS results also confirm that CW exhibits excellent charge transfer ability (Fig. S7). Then, photoelectrochemical (PEC) experiments over CW were performed under 365 or 940 nm light (Fig. 6b). All the yields increase with the time being and the UV H_2 evolution and NIR NH_3 generation show sharper rise. After 15 h, the yields of H_2 are 2535.0 nmol (365 nm) and 17.0 nmol (940 nm), while that of NH_3 are 279.0 nmol (365 nm) and 121.5 nmol (940 nm), respectively. The PEC NH_3 generation rates are 18.6 nmol/h (365 nm) and 8.1 nmol/h (940 nm), while the H_2 evolution rates are 169.0 nmol/h (365 nm) and 1.1 nmol/h (940 nm), respectively. H_2 evolution rates are 9.1 and 0.1 times higher than NH_3 generation rates under UV and NIR light irradiation. Compared with that using UV light, the efficiency of NIR induced PEC NH_3 generation has been improved greatly, owing to the limitation of LSPR by which only N_2 fixation reaction can be improved, similar to the result in the above photocatalytic reaction. The photoelectrochemical results also indicate the importance of electron.

Then, DFT method with ωB97X-D/6-31G(D)* basis set was carried out to optimize the geometry and frequency of vacancy-rich (V-rich) and pristine g-C_3N_4 (Fig. 7a and S8). Three zones are chosen as potential active sites waiting for N_2 molecule insertion. As indicated in Table S8, the two g-C_3N_4 show the same adsorption energy trend as A > B > C, owing to the strong interaction and proper space in zone A. A notable increase of adsorption energy can be observed after O atoms or hydroxyl groups introduced into CN skeleton. After protonation, the adsorption energy value becomes 3.0 times in zone A and 2.3 times in zone B as great. But no obvious difference is observed in zone C, ascribing to the same structure. The results confirm that the vacancies can provide adsorption active sites to activate N_2. More detailed information for geometry optimizing and adsorption energy calculation are shown in Table S9.

Gibbs free energy in N_2 fixation over two g-C_3N_4 samples was also investigated (Fig. 7b). More details about g-C_3N_4 related geometry optimizing are shown in Fig. S10. Compared with pristine one, V-rich g-C_3N_4 exhibits a lower Gibbs free energy in the whole process, suggesting its higher catalytic activity [29]. The first step of N_2 fixation reaction is the most difficult in the whole reaction procedure, exhibiting non-spontaneous adsorption behavior over both two g-C_3N_4. An obvious decrease of free energy can be found in the proton transfer reaction (from NNH to $NHNH_2$) over V-rich g-C_3N_4. The reaction energies of these two steps for V-rich g-C_3N_4 are calculated to be −0.82 and −0.14 eV while −0.93 and −0.52 eV in pristine g-C_3N_4 respectively. However, few difference of energy occurs between these two g-C_3N_4 in the last two reaction step, with the reaction energy of −0.53 and

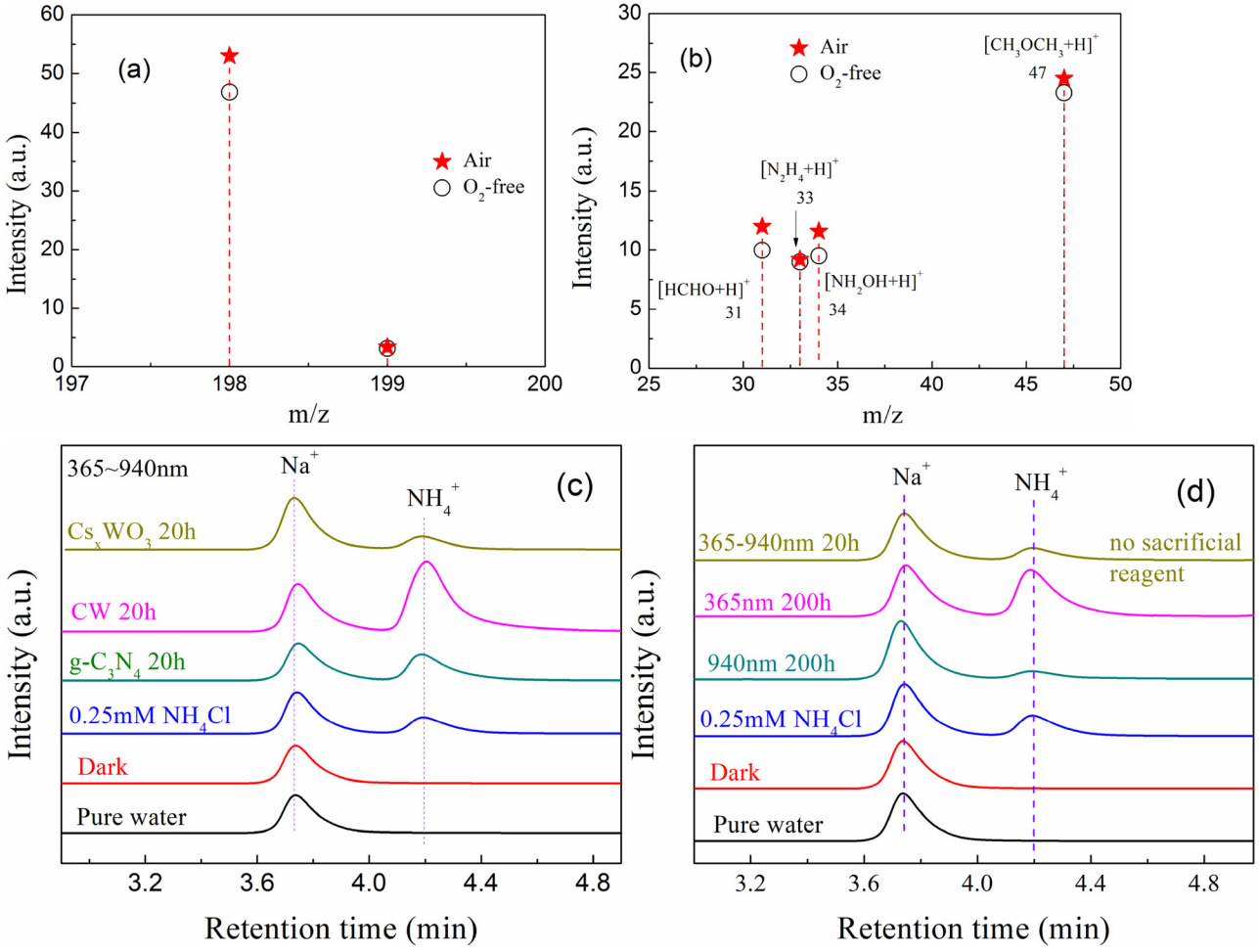

Fig. 5. Mass spectra of the (a) indophenol and (b) reaction solution over CW photocatalyst; Ion chromatography spectrum of reaction solution over (c) CW, g-C_3N_4 and Cs_xWO_3 photocatalyst under full spectrum light irradiation, and (d) CW photocatalyst.

−0.66 eV for pristine g-C_3N_4 and −0.50 and −0.64 eV for V-rich one. The results reveal that V-rich g-C_3N_4 exhibits better proton transfer ability as well as N_2 adsorption ability [19].

In addition, it is important to investigate the nitrogen source of NH_3 during N_2 fixation reaction over CW photocatalyst. First, N_2 fixation reaction was performed in the dark and N_2 atmosphere with different temperature. As shown in Table 1, little NH_3 generation was observed. However, the production of NH_3 greatly increased in the room temperature under full spectrum light irradiation. It indicates the crucial importance of light irradiation and the certain thermal stability of CW photocatalyst. Second, the same reaction was carried out in Ar atmosphere under full spectrum light irradiation. The results show that the

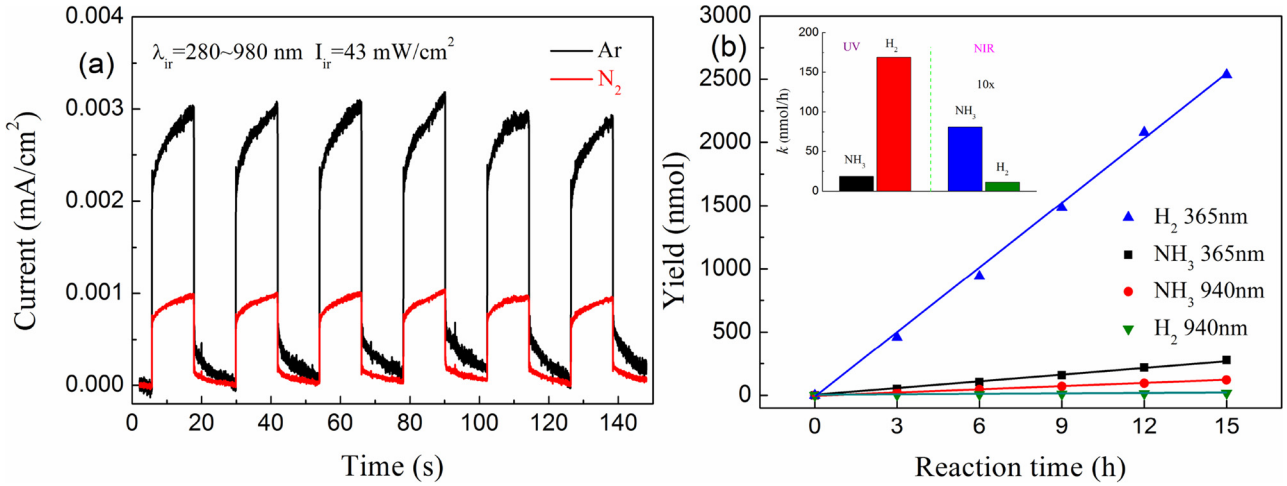

Fig. 6. (a) Photocurrent response under full spectrum light in Ar or N_2 gas and (b) Photoelectrochemical NH_3 and H_2 generation under 365 or 940 nm light irradiation over CW photoelectrode.

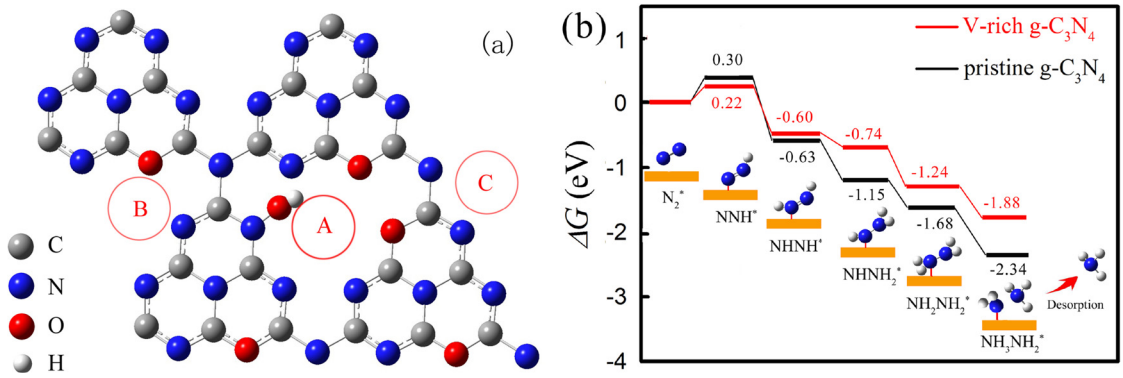

Fig. 7. Theoretical prediction of (a) N_2 adsorption on V-rich g-C_3N_4 at different zones and (b) Free energy change in the reaction procedure. (A)–(C): potential adsorption sites.

Table 1
Photocatalytic N_2 fixation over CW composite.

N_2 fixation			
Light (nm)	Temp. (K)	Air	NH_3 Yield (umol h^{-1} g^{-1})
dark	293	N_2	0.010
dark	313	N_2	0.011
dark	333	N_2	0.012
365–940	298	N_2	331
365–940	298	Ar	3.2

Table 2
LC–MS analysis summary.

LC–MS		
Indophenol addition	m/z	peak
No	33	$[N_2H_4 + H]^+$
No	34	$[NH_2OH + H]^+$
Yes	198	^{14}N-indophenol anion
Yes	199	^{15}N-indophenol anion

Table 3
Elemental content ananlysis.

Elemental content (%)	Fresh catalysts	Used catalysts
C	24.54	24.37
N	13.30	13.35
Cs	7.35	7.32
W	31.08	31.02
O	21.60	21.71
H	2.13	2.23

NH_3 generation rates are 331 μmol h^{-1} g^{-1} in N_2 atmosphere and 3.2 μmol h^{-1} g^{-1} in Ar. The huge difference of NH_3 production between the presence and absence of N_2 atmosphere confirms that N_2 is the nitrogen source of NH_3. In addition, LC–MS measurement was also performed to monitor the production of N_2 fixation reaction. The results of Fig. 5 were summarized in Table 2. As mentioned before, no impurity *m/z* peaks were observed in the LC–MS analysis, indicating the stability of CW in the photocatalytic N_2 fixation. It is worth mentioning that the existence of $^{15}N_2$ signal further illustrates the N_2 gas is the nitrogen source. In addition, to further study the stability of CW photocatalyst, the elemental analysis was also employed before and after ten times repeated N_2 fixation reactions over CW. As shown in Table 3, no obvious differences can be observed between the fresh and used CW in the elemental analysis. The slight increase in the content of N, H and O could be caused by the absorption of NH_3 or other oxide species on the surface. Therefore, no nitrogen left the CW photocatalyst to form NH_3 in the N_2 fixation.

4. Conclusion

In summary, we demonstrate that atmospheric N_2 can be efficiently reduced to NH_3 by g-C_3N_4/Cs_xWO_3 composite under full-spectrum light, without any precious metal cocatalysts. Along with the visible light activity of g-C_3N_4 and the NIR light absorption of Cs_xWO_3, the designed vacancies could activate N_2 and significantly promote the interfacial electron transfer. The N_2 fixation rate of CW in this study was high in different light irradiation and selectivity towards NH_3 over H_2 is realized by using NIR light. UV-NIR light synergistic effect can improve the photocatalytic N_2 fixation largely. Above all, with the proper control of methanol, O_2 plays a positive role in ammonia synthesis. It is like that a good horse always needs a good spur. With the protection of a sacrificial agent, the produced NH_3 will not be oxidized. However, excess sacrificial agent will expend excessive amount of active species, then it does not have enough species to prepare ammonia. A proper sacrificial agent is very important. Since O_2 and sacrificial agent are common presence, the present finding of their relationship in formation of the final product as a promoter might be stimulating for other catalytic reactions.

Acknowledgements

This research was supported by the National Natural Science Foundation of China (51402139). Thanks to the partial supporting from the JSPS KAKENHI Grant Number JP16H06439 (Grant-in-Aid for Scientific Research on Innovative Areas), the Dynamic Alliance for Open Innovation Bridging Human, Environment and Materials, the Cooperative Research Program of “Network Joint Research Center for Materials and Devices”.

Appendix A. Supplementary data

Supplementary material related to this article can be found, in the online version, at doi:https://doi.org/10.1016/j.apcatb.2018.04.081.

References

[1] (a) A.J. Medford, M.C. Hatzell, ACS Catal. 7 (2017) 2624–2643;
(b) G. Schrauzer, T. Guth, J. Am. Chem. Soc. 99 (1977) 7189–7193;
(c) Y. Zhao, Y. Zhao, G. Waterhouse, L. Zheng, X. Cao, F. Teng, L. Wu, C. Tung, D. Hare, T. Zhang, Adv. Mater. 29 (2017) 1703828;
(d) C. Guo, J. Ran, A. Vasileff, S. Qiao, Energy Environ. Sci. 11 (2018) 45–56.
[2] (a) Y.T. Liang, B.K. Vijayan, K.A. Gray, M.C. Hersam, Nano Lett. 11 (2011) 2865–2870;
(b) D. Zhu, L. Zhang, R.E. Ruther, R.J. Hamers, Nat. Mater. 12 (2013) 836–841.
[3] K. Ranjit, T. Varadarajan, B. Viswanathan, J. Photochem. Photobiol. A 96 (1996) 181–185.

[4] T. Oshikiri, K. Ueno, H. Misawa, Angew. Chem. Int. Ed. 55 (2016) 3942–3946.
[5] (a) G.H. Dong, W.K. Ho, C.Y. Wang, J. Mater. Chem. A3 (2015) 23435–23441;
(b) H. Li, J. Shang, Z.H. Ai, L.Z. Zhang, J. Am. Chem. Soc. 137 (2015) 6393–6399;
(c) D. Bao, Q. Zhang, F. Meng, H. Zhong, M. Shi, Y. Zhang, J. Yan, Q. Jiang, X. Zhang, Adv. Mater. 29 (2016) 1604799;
(d) H. Yu, R. Shi, Y. Zhao, T. Bian, Y. Zhao, C. Zhou, G.I.N. Waterhouse, L. Wu, C. Tung, T. Zhang, Adv. Mater. 29 (2017) 1605148.
[6] (a) S. Hu, X. Chen, Q. Li, F. Li, Z. Fan, H. Wang, Y. Wang, B. Zheng, G. Wu, Appl. Catal. B: Environ. 201 (2017) 58–69;
(b) H. Li, J. Shang, J.G. Shi, K. Zhao, L.Z. Zhang, Nanoscale 8 (2016) 1986–1993;
(c) L. Lin, H. Ou, Y. Zhang, X. Wang, ACS Catal. 6 (2016) 3921–3931.
[7] (a) H. Hirakawa, M. Hashimoto, Y. Shiraishi, T. Hirai, J. Am. Chem. Soc. 139 (2017) 10929–10936;
(b) H. Zhao, X. Ding, B. Zhang, Y. Li, C. Wang, Sci. Bull. 62 (2017) 602–609.
[8] X. Huang, G. Zhao, G. Wang, J. Mater. Chem. A 5 (2017) 24631–24635.
[9] A. Shi, H. Li, S. Yin, B. Liu, J. Zhang, Y. Wang, Appl. Catal. B: Environ. 218 (2017) 137–146.
[10] G. Li, C. Guo, M. Yan, S. Liu, Appl. Catal. B: Environ. 183 (2016) 142–148.
[11] (a) F. Cheng, H. Wang, X. Dong, Chem. Commun. 51 (2015) 7176–7179;
(b) J. Liu, Q. Xu, F. Shi, S. Liu, J. Luo, L. Bao, X. Feng, Appl. Surf. Sci. 309 (2014) 175–180.
[12] B. Wiley, S. Im, Z. Li, J. MecLellan, A. Siekkinen, Y. Xia, J. Phys. Chem. B 110 (2006) 15666–15675.
[13] T.M. Mattox, A. Bergerud, A. Agrawal, D.J. Milliron, Chem. Mater. 26 (2014) 1779–1784.
[14] J. Choi, K. Moon, I. Kang, S. Kim, P.J. Yoo, K.W. Oh, J. Park, Chem. Eng. J. 281 (2015) 236–242.
[15] W. Ong, L. Tan, S. Chai, S. Yong, A. Mohamed, Nano Energy 13 (2015) 757–770.
[16] J. Chen, D. Yu, W. Liao, M. Zheng, L. Xiao, H. Zhu, M. Zhang, M. Du, J. Yao, ACS Appl. Mater. Interfaces 8 (2016) 18132–18139.
[17] Z. Huang, F. Li, B. Chen, G. Yuan, Catal. Sci. Technol. 6 (2016) 2942–2948.
[18] K. Xu, H. Ding, M. Zhang, M. Chen, Z. Hao, L. Zhang, C. Wu, Y. Xie, Adv. Mater. 29 (2017) 1606980.
[19] J. Rittle, J.C. Peters, J. Am. Chem. Soc. 139 (2017) 3161–3170.
[20] Y.I. Kim, S.J. Atherton, E.S. Brigham, T.E. Mallouk, J. Phys. Chem. 97 (1993) 11802–11810.
[21] K. Hoshino, Chem. Eur. J. 7 (2001) 2727–2731.
[22] C.G. Zhan, J.A. Nichols, D.A. Dixon, J. Phys. Chem. A 107 (2003) 4184–4195.
[23] M.G. Walter, E.L. Warren, J.R. Mckone, S.W. Boettcher, Q. Mi, E.A. Santori, N.S. Lewis, Chem. Rev. 110 (2010) 6446–6473.
[24] (a) Y. Zhang, K. Ueno, Y. Mori, X. Shi, T. Oshikiri, K. Murakoshi, H. Inoue, H. Misawa, Angew. Chem. Int. Ed. 53 (2014) 10350–10354;
(b) Y. Zhang, K. Ueno, Y. Mori, T. Oshikiri, H. Misawa, J. Phys. Chem. C 119 (2015) 8889–8897;
(c) W. Guo, C. Guo, N. Zheng, T. Sun, S. Liu, Adv. Mater. 29 (2017) 1604157;
(d) J.M.P. Martirez, E.A. Carter, ACS Nano 10 (2016) 2940–2949.
[25] D.J. Martin, P.J.T. Reardon, S.J.A. Moniz, J. Tang, J. Am. Chem. Soc. 136 (2014) 12568–12571.
[26] W. Zhao, J. Zhang, X. Zhu, M. Zhang, J. Tang, M. Tan, Y. Wang, Appl. Catal. B: Environ. 144 (2014) 468–477.
[27] L. Cao, X. Li, L. Fan, L. Zheng, M. Wu, S. Zhang, Q. Huang, Mar. Drugs 15 (2017) 51.
[28] X. Li, W. Wang, D. Jiang, S. Sun, L. Zhang, X. Sun, Chem. Eur. J. 22 (2016) 13819–13822.
[29] (a) L.M. Azofra, D.R. MacFarlane, C. Sun, Phys. Chem. Chem. Phys. 18 (2016) 18507–18514;
(b) H. Choi, Y. Park, Y. Kim, Y. Lee, J. Am. Chem. Soc. 133 (2011) 2084–2087.